ADVANCED FUNCTIONAL MATERIALS
www.afm-journal.de

Facile Synthesis of Cu_xS Electrocatalysts for CO_2 Conversion into Formate and Study of Relations Between Cu and S with the Selectivity

Sasho Stojkovikj, Gumaa A. El-Nagar, Siddharth Gupta, Metodija Najdoski, Violeta Koleva, Theocharis Tzanoudakis, Frederik Firschke, Peter Bogdanoff, and Matthew T. Mayer**

The conversion of CO_2 into formate ($HCOO^-$), a techno-economically feasible product, can be achieved using earth-abundant Cu_xS electrocatalysts, but questions remain regarding how catalyst structure, composition, and reaction environment influence product selectivity. A novel synthesis method based on electrodeposition of Cu foam and its subsequent sulfidation via immersion in sulfur saturated toluene solution resulted in Cu_xS foams. Catalytic activity studies found that $HCOO^-$ selectivity is dependent on electrochemical activation at higher overpotentials. To understand the effects of activation, determine the active forms of the catalysts, and identify the role of sulfur, the electrodes are carefully characterized as well as gaseous and sulfur dissolved in electrolyte. This included study of the effects of intentional addition of solution sulfur species, identification of the sulfur loss, determination of the electrode composition and relating sulfur speciation to observed product selectivity. It is found that residual sulfur stabilizes Cu^+ during electrolysis at potentials favoring $HCOO^-$ production, in contrast to pristine Cu that undergoes complete reduction and shows poor $HCOO^-$ selectivity. Sulfur in both the catalyst and dissolved in electrolyte are of dynamic nature, and surface residues of SO_4^{2-} species are identified in all activated catalysts which correspond with enhanced $HCOO^-$ production.

1. Introduction

The emission of the greenhouse gas CO_2 in the atmosphere is continuously increasing together with the energy demand that is still majorly derived from fossil fuels, caused by the development of the global society since the start of the industrial revolution.[1,2] Significant long-term measures are already taken in the past decades to mitigate the CO_2 emissions via decreasing the dependence from fossil fuels energy production,[3,4] however more immediate actions are necessary. A core component of a carbon-neutral economy will be efficient renewable energy driven CO_2 capture and its conversion into valuable products for use as fuels and chemicals in the existing industry, substituting fossil-derived chemicals.[3,4] The electrochemical conversion of CO_2 (CO_2EC) is a promising approach for CO_2 recycling into value-added products,[4] and among the wide range of possible products, to date the 2 e^- CO_2EC

S. Stojkovikj, G. A. El-Nagar, S. Gupta, T. Tzanoudakis, F. Firschke, M. T. Mayer
Helmholtz Young Investigator Group: Electrochemical Conversion
Helmholtz-Zentrum Berlin für Materialen und Energie GmbH
Hahn-Meitner-Platz 1, D-14109 Berlin, Germany
E-mail: saso.stojkovik@ugd.edu.mk; m.mayer@helmholtz-berlin.de

S. Stojkovikj, S. Gupta, T. Tzanoudakis
Institut für Chemie und Biochemie
Freie Universität Berlin
Arnimallee 22, D-14195 Berlin, Germany

The ORCID identification number(s) for the author(s) of this article can be found under https://doi.org/10.1002/adfm.202415405

DOI: 10.1002/adfm.202415405

S. Stojkovikj
Faculty of Technology
Goce Delcev University
Krste Misirkov 10-A, Stip 2000, Republic of North Macedonia

M. Najdoski
Institute of Chemistry
Faculty of Natural Sciences and Mathematics
Ss Cyril and Methodius University Skopje
Arhimedova 5, Skopje 1000, Republic of North Macedonia

V. Koleva
Institute of General and Inorganic Chemistry
Bulgarian Academy of Sciences
Acad. G. Bonchev Str. Bldg. 11, Sofia 1113, Bulgaria

P. Bogdanoff
Institute of Solar Fuels
Helmholtz-Zentrum Berlin für Materialen und Energie GmbH
Hahn-Meitner-Platz 1, D-14109 Berlin, Germany

products CO and formic acid/formate ($HCOOH/HCOO^-$) are closest to being techno-economically viable for possible large-scale production.[3–5] Among metal catalysts explored for CO_2EC, only Cu is capable of significantly reducing CO_2 beyond CO in multielectron steps to produce high-value products like hydrocarbons, alcohols, etc.[1,3,6,7] but it unfortunately suffers from selectivity issues requiring additional costly product separation steps,[8] hence necessitating further development to reach feasibility. In the shorter term, understanding and controlling the catalytic processes during CO_2EC into the most techno-economically viable 2 e- products is of great importance for initial implementations of the technology. In particular, HCOOH and $HCOO^-$ salts are important feedstock chemicals used in broad industrial fields.[9] Moreover, there are significant research efforts to develop fuel cells that can efficiently run on formate which would provide advantages over H_2 in terms of safety, storage and transportation issues.[4,10] Several elements (Cd, In, Sn, Hg, Tl, Pb, Bi)[11] and their combinations (Sn-Pb, Cu-Sn, Cu-In, Cu-Pb, Cu-Pb-Sn, Cu-S etc.),[11–16] have been investigated as electrocatalysts for CO_2EC into $HCOO^-$. However, among them only Cu, Sn, In, Bi and S are not highly toxic and all of them except S are relatively rare in Earth's crust, and moreover are listed as elements with certain risk of future supply.[17,18] Comparatively speaking, Cu is more abundant[19] and cheaper[20] than Sn, In and Bi. Hence, combining Cu with S in various copper sulfide (Cu_xS) based electrocatalysts appears to be a very suitable route to CO_2 conversion into $HCOO^-$. Namely, those materials have already emerged as attractive candidates for this purpose.[16,21–33] Cu_xS can be synthesized using numerous methods.[16,30–41] Under negative potentials applied during CO_2EC, these materials are expected to significantly transform (therefore are sometimes referred as sulfide-derived,[28,42] doped[33,43] or modified[44] Cu). This typically comes with significant reduction of Cu and loss of S, but nevertheless exhibits high $HCOO^-$ selectivity in contrast to what is commonly observed on metallic and oxide-derived Cu.[1,3,6,7] Regarding the $HCOO^-$ production mechanism, it has been proposed that the presence of persistent residual sulfur may stabilize the Cu^+ specie on the catalyst surface and favors the binding of the *OCHO* intermediate which transforms into $HCOO^-$ following a second electron transfer step.[21,23,26,29,31,33] Moreover, it was found that the presence of sulfur coincides with suppression of the undesired hydrogen evolution reaction (HER).[33] While several studies indicated that Cu is either partially oxidized or sulfur remains persistent in the structure of Cu under CO_2 electrolysis conditions,[21,24,28–30,33,42] to the best of our knowledge there is no conclusive evidence whether under operating conditions the surface Cu is fully reduced to metallic or remains partially oxidized. Therefore, in this study we sought to address this question via study of the chemical nature of surface Cu and S under near operating conditions. For this purpose, the electrocatalysts were examined with x-ray photoelectron spectroscopy (XPS) after conducting both the electrolysis and transfer of the samples to the analyzer under inert atmosphere to prevent air-induced oxidation when the electrochemical bias is removed (referred as "quasi in situ XPS"[45–47]). By tracking the sulfur loss from the electrocatalyst under reductive electrochemical bias, its dissolution in the electrolyte and its possible effects on the selectivity were investigated in the scope of this study. We decided to develop and utilize rather very fast, simple, cheap, and reproducible method under mild conditions to prepare a CO_2 to $HCOO^-$ conversion electrocatalyst with decent selectivity. Moreover, we sought to avoid usage of hazardous sulfur compounds (H_2S, S^{2-} salts, thiourea etc.) or expensive ionic liquids as precursors. Cu foam was prepared via dynamic hydrogen bubble template (DHBT) electrodeposition,[47] which was subsequently sulfidated by immersion into sulfur dissolved in toluene leading to formation of Cu_xS foam. All synthesized materials were examined to reveal their chemical composition, structure, morphology, and surface speciation. Examining the Cu_xS foam for its CO_2 conversion electrocatalytic activity, it was revealed that the besides the $HCOO^-$ selectivity being dependent on the applied potential it is also dependent whether the material is subjected to electrochemical activation. Whether this phenomenon is affected by the bulk and/or surface composition and speciation of the Cu and S in the catalyst and the dynamic loss/redeposition of sulfur species in/from the electrolyte, is first briefly presented in Scheme 1 and later thoroughly discussed based on the results from various experiments conducted in the scope of this research.

2. Results and Discussion

The main findings in the scope of this research are presented in Scheme 1 and briefly discussed in the four points below, where each point represents an experimental step in the research process. As a summary, invariant of the sample type, it was generally found that the surface of the Cu_xS foam electrode should contain ≤30 at.% total sulfur and the electrolyte ≤0.3 $mg{\cdot}dm^{-3}$ dissolved sulfur species in order to achieve ≥50% faradaic efficiency (FE) for CO_2 to $HCOO^-$ conversion.

(I) Process of DHBT electrodeposited Cu foam sulfidation via sulfur dissolved in toluene – synthesis of Cu_xS foam electrocatalyst with digenite/roxbyite mixed phase composition. A facile sulfidation method is developed in this study.

(II) The electrochemical reduction of the Cu_xS foam electrocatalyst is leading to formation of residual sulfur stabilized Cu^+ active surface sites that are favoring $HCOO^-$ production (compared to pristine Cu). The electrochemically activated catalysts at −0.9 V show better performance in CO_2 to $HCOO^-$ conversion when examined at −0.7 V. Additionally SO_4^{2-} are found on the surface in all activated catalysts and this specie can be considered as a descriptor relating to the electrochemical activation.

(III) Re-examining the activated electrocatalysts in fresh electrolyte shows better performance for CO_2 to $HCOO^-$ conversion at −0.9 V while almost the same at −0.7 V.

(IV) When surface of pristine Cu foam is immersed in electrolyte containing dissolved sulfur species (obtained via previous reduction of Cu_xS foam) and activated at −0.9 V (abbreviated as Cu+S foam), it shows similar structure-activity relations and $HCOO^-$ production performance as in the case of the activated Cu_xS foam that is re-examined in fresh electrolyte (Cu_xS foam-NE).

Detailed discussion of the experimental observations and interpretations are provided in the following sub-sections of Section 3.

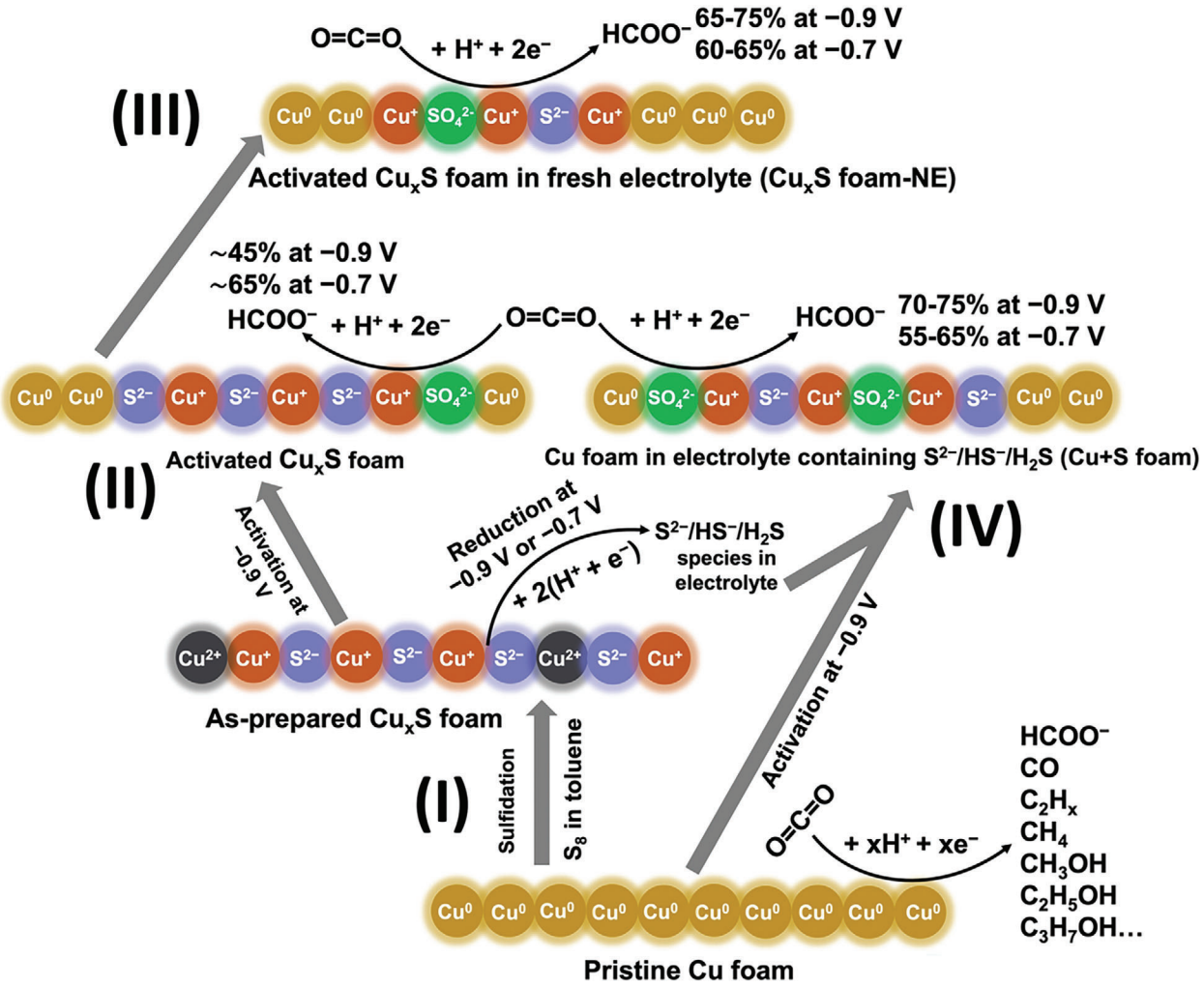

Scheme 1. Representation of the catalyst materials, testing conditions, and selectivity observations to summarize the overall catalyst-electrolyte composition-activity relations in Cu_xS electrocatalysts for CO_2 conversion.

2.1. Characterization of the Synthesized Material

Cu with foam-like morphology was electrodeposited on Cu mesh substrates via DHBT method,[47] as depicted in Figure S1 (Supporting Information) and described above in the experimental section and additionally in Section S1.2. (Supporting Information). The Cu foam consists of typical dendrite structures arranged as interconnected pores and channels (**Figures 1a** and S3, Supporting Information) that were formed during the electrodeposition, with pore size of ≈30 µm and thickness of ≈40 µm (see Figure S4a and Table S2, Supporting Information). The method for Cu foam sulfidation is based on a direct reaction between elemental Cu and sulfur dissolved in toluene at room temperature. The sulfidation process only occurs when metallic Cu is exposed to dissolved reactive sulfur species, therefore an initial acidic etching step was necessary prior to sulfidation to remove native surface species (e.g., oxides, hydroxides and carbonates) which passivate the surface, as discussed in Section S1.3. (Supporting Information). The sulfidation process did not significantly affect the bulk morphology, thus the pore sizes and thickness are preserved (see Figures 1 and S4, S5, and Table S2, Supporting Information) although blunting of the dendrite edges can be observed (cf. Figure 1a with Figures 1b and S3c with Figure S5c, Supporting Information). The energy-dispersive X-ray spectroscopy (EDX) mapping shows homogeneous distribution of Cu and S throughout the sulfidated foam with nominal sulfur fraction of ≈30 at.% (Cu:S atomic ratio ≈2), as presented in Figure S5d,e (Supporting Information). From the X-ray diffraction (XRD) analysis results (Figures 1c and S6, Supporting Information) it was found that the Cu foam with polycrystalline Cu structure during the sulfidation procedure transforms into copper sulfide with mixed phase composition which corresponds to digenite $Cu_{1.765}S$ as a predominant (≈70 wt.%) and roxbyite Cu_7S_4 as a secondary phase. Both phases resemble Cu_xS stoichiometry where x = 1.7–1.8, and the sulfidation reaction can be described with Equation (1).[22]

$$xCu + S \rightarrow Cu_xS\ (\text{digenite/roxbyite phase}),\quad x = 1.7 - 1.8 \quad \Delta_f G^\circ = -53.6\,\text{kJ}\cdot\text{mol}^{-1} \tag{1}$$

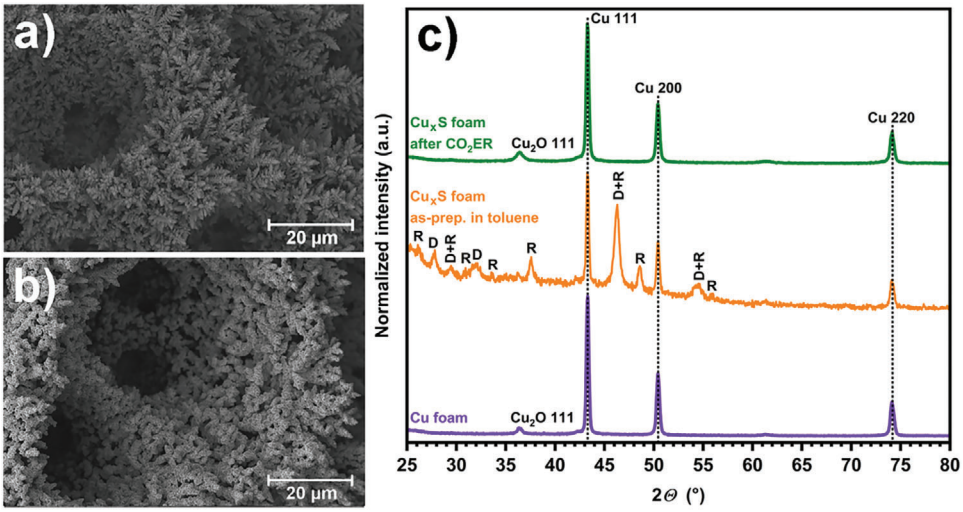

Figure 1. Scanning electron microscopy (SEM) images of a) Cu foam and b) Cu_xS foam composed of dendrite microstructures. c) GI-XRD patterns of Cu foam and sulfidized Cu foam. Peaks due to Cu-S phases are labelled according to the reflections in the corresponding database patterns for (D) digenite $Cu_{1.765}S$ (ICDD PDF 2-023-0960) and (R) roxbyite Cu_7S_4 (ICDD PDF 2-023-0958). Vertical dashed lines correspond to the metallic Cu substrate.

From an environmental point of view, the sulfur/toluene solution can be reused for the synthesis purpose after adjusting the sulfur concentration to maintain saturation level which contributes to minimizing the amount of required solvent. Besides toluene, synthesis of Cu_xS was also performed using CS_2 as a sulfur solvent. The material prepared in CS_2 showed similar phase composition (XRD results in Figure S6, Supporting Information). Furthermore, the materials prepared in both solvents (as powders via sulfidation of Cu foil) showed similar thermal properties when studied with thermogravimetric analysis (TGA) (Figure S7a,b, Supporting Information) coupled with mass spectrometry (MS) in situ to follow the gaseous product evolution (Figure S7c,d, Supporting Information) and differential scanning calorimetry (DSC) (Figure S7e,f, Supporting Information). These thermal behavior similarities are likely caused by their similar chemical composition, yet there are discrepancies in the literature whether those thermal transformations are exothermic,[48] as observed from our results (Figure S7e,f, Supporting Information), or endothermic.[49,50] More thorough discussion of the TGA-MS and DSC results is provided in Section S1.4. (Supporting Information). We note that the material synthesized in CS_2 was only studied for its chemical composition, structure and thermal properties, and not subjected to additional examination due to the hazardous nature of CS_2 which we thereafter sought to avoid. Thus, all other studies were conducted using toluene as synthesis solvent.

The Cu foam was not the first choice for a Cu substrate that is supposed to be subsequently sulfidated. Namely, we initially started by sulfidation of Cu foil via immersing it in solution containing sulfur dissolved in toluene. It was found that the obtained material resembles the same phase composition as in the case of Cu_xS foam (Figure S6, Supporting Information). However, the as-prepared Cu_xS coating readily delaminated from the surface of the foil (Figure S8, Supporting Information). Similar mechanical instability was observed when bare Cu mesh (without subsequent electrodeposition of Cu foam) was used as a substrate (see Figure S9 and Section S1.3., Supporting Information). In our case, to overcome this problem, microporous Cu foam was deposited on the mesh substrate and subsequently sulfidated, as described above, which resulted in superior stability under electrocatalytic conditions. We note that direct reactions between elemental Cu and sulfur dissolved in organic solvents, e.g., benzene and $CHCl_3$ are reported in the literature,[40,41] but nevertheless those are more hazardous than the toluene used here.

2.2. Electrocatalytic Activity for CO_2 Conversion

The Cu_xS foam electrodes prepared as described above generally produced $HCOO^-$ with high selectivity (expressed as faradaic efficiency, FE) across a range of conditions, along with negligible yields of other CO_2EC products (≤3% FE), as presented in **Figures** 2a–c and S10 (Supporting Information). This is in stark contrast to the electrocatalytic activity of pristine Cu foam samples without sulfur which produce a mixture of products typical for Cu with dendrite morphology[6,45] (see Figures 2d–f and S11, Supporting Information) and shows the significant selectivity shift resulting from sulfidation of Cu foam. These results are generally in accordance with several past studies for Cu_xS based electrocatalysts.[16,21–27,32,33]

CO_2EC electrocatalysts are typically studied across a range of applied potentials, usually by stepping from low to high overpotential (hence, negative direction), to determine potential-dependent catalytic activity. Knowing that Cu compounds are expected to transform significantly under electrochemical reduction conditions, we sought to study in more detail the specific influences of sample activation and testing sequence on the observed selectivity, and therefore examined the Cu_xS foam electrodes in the potential range between –0.5 and –0.9 V (potentials are reported vs RHE herein, unless otherwise noted) via stepping the applied potential in different directions. Stepping in the negative direction (from –0.5 to –0.9 V) is abbreviated as ND and stepping in positive direction (from –0.9 to –0.5 V) as PD (indicated with arrows in Figures 2 and S10, Supporting

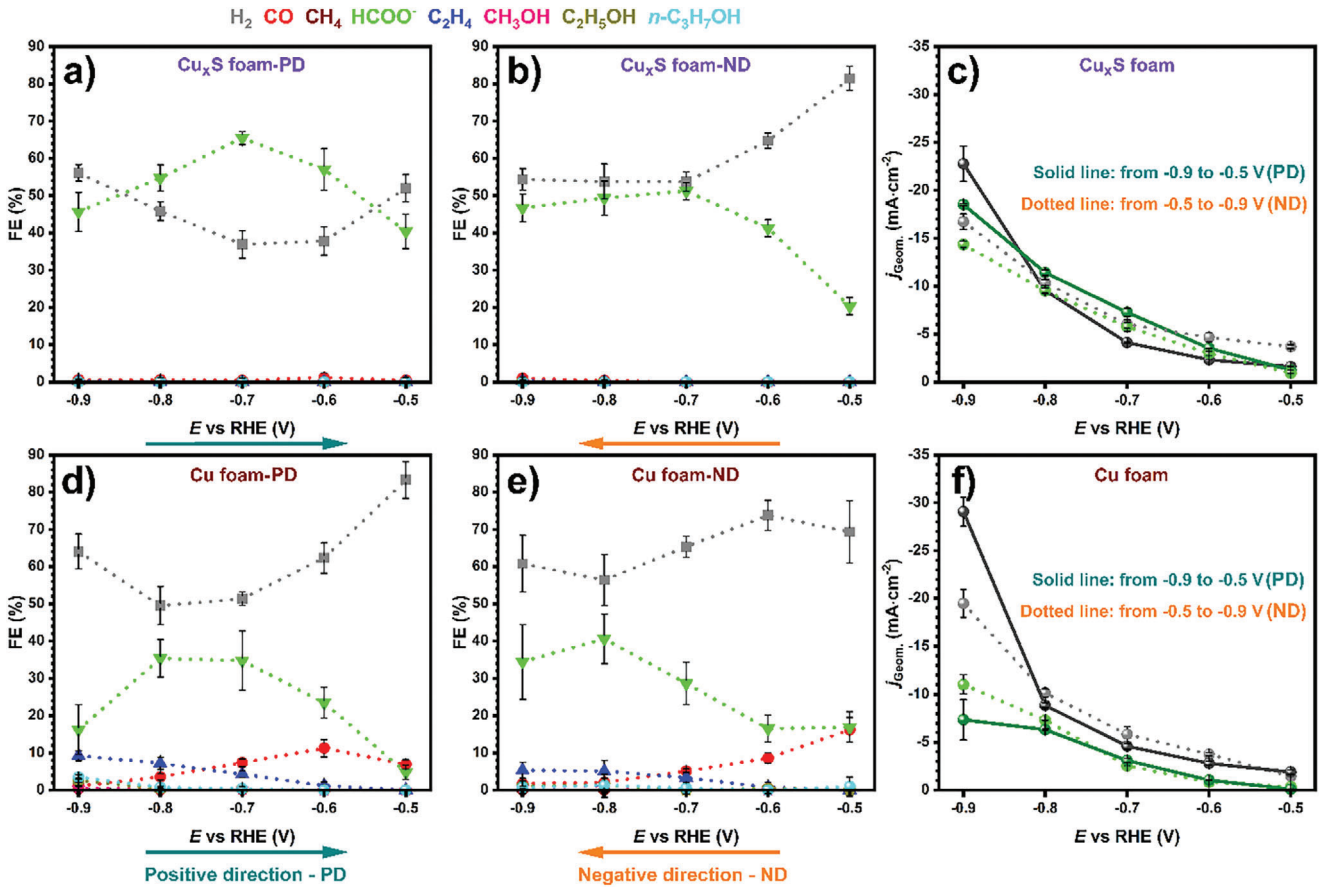

Figure 2. Distribution of FE for H_2 and various CO_2EC products (legend on top) and partial current densities for H_2 and $HCOO^-$ obtained on Cu_xS foam and pristine Cu foam electrocatalysts during 1 h electrolysis at each potential: FE distribution obtained with stepping the potential in positive direction (PD) for Cu_xS foam a) and pristine Cu foam d); FE distribution examined with stepping the potential in negative direction (ND) for Cu_xS foam b) and pristine Cu foam e). The arrows point the direction of stepping of the applied potential. Partial current densities for H_2 (dark and light grey lines) and $HCOO^-$ (dark and light green lines) obtained when stepping the potential in PD (solid line) and ND (dotted line) for Cu_xS foam c) and pristine Cu foam f).

Information). According to the results, $HCOO^-$ production peaks at –0.7 V regardless of the stepping direction, yet the selectivity is higher in the case of stepping in PD (FE ≈65% and j_{HCOO^-} = –7.3 mA•cm^{-2} in PD vs FE ≈ 50% and j_{HCOO^-} = –5.7 mA•cm^{-2} in ND). Consequently, at –0.7 V the hydrogen evolution reaction (HER) is most suppressed under positive potential stepping sequence (FE_{H2} ≈35%, j_{H2} = –4.1 mA•cm^{-2}), while the FE_{HCOO^-} is practically equal to FE_{H2} when stepped in ND (cf. Figure 2a,b). At potentials at –0.9 and at –0.8 V when stepped in ND, the differences between FE_{HCOO^-} and FE_{H2} are small, but in favor of the HER which dominates at –0.6 and –0.5 V. However, regardless of the direction of the potential stepping sequence, no difference is observed between the FEs_{HCOO^-} (≈45%) at –0.9 V and accordingly the same applies for the FEs_{H2} (≈55%), again comparing Figure 2a with Figure 2b. Stepping direction effects on the selectivity are also observed in the case of bare Cu foam (Figure 2d with Figure 2e). It appears that an electrochemical activation under high overpotential induces the enhancement in FE_{HCOO^-} when the Cu_xS foam electrodes are initially subjected to –0.9 V. Whether this phenomenon comes intrinsically from the presence of sulfur or is related to possible surface roughness effects on the materials (since it is observed both for bare and sulfidated Cu foam), will be discussed in the following paragraph.

The estimation of relative surface roughness (Figure S12 and Table S3, Supporting Information) showed comparable values measured after electrolysis for bare Cu- (at –0.9 V) and Cu_xS foams (at –0.9 V and at –0.7 V), which suggests that the FE_{HCOO^-} enhancement does not arise simply from roughness factor differences. The dendrite microstructures composing the Cu_xS foam composed of dendrites underwent transformation into sponge-like features, regardless of the direction of stepping the applied potential (see Figures S13a–c–S22a–c, Supporting Information), while the pristine Cu foam subjected to –0.9 V maintains similar dendrite features as in the pre-electrolysis samples (cf. Figure S3a–c with Figure S23a–c, Supporting Information). This transformation of the dendrite microstructures in the case of Cu_xS foam was found to occur only when negative electrochemical bias is applied but not under open circuit conditions when the sample is immersed in the electrolyte (Figure S24a–c, Supporting Information). The reason for such morphological transformation can be explained by the sulfur loss as H_2S both from the bulk and surface of the Cu_xS foam

during the electrochemical reduction, as discussed in the next subsection.

Up to now it is clear that the presence of sulfur typically enhances the $HCOO^-$ production and suppresses the HER and other CO_2EC products, and this is most pronounced when the Cu_xS foam electrodes are initially activated at –0.9 V. In order to further investigate this phenomenon, a series of experiments were conducted. First, we started with testing the electrochemical activation via directly examining the Cu_xS foam electrocatalyst at applied potential of –0.7 V under various conditions, as presented in Figure S25 (Supporting Information) (see Table S1, Supporting Information for experimental conditions). Examining the electrocatalyst directly at –0.7 V showed very small difference in favor of enhancing the FE_{HCOO^-} over FE_{H2} in comparison when the activity is measured at the same potential after stepping in negative direction (ND). On the other hand, the total current density is somewhat higher than in the case when the material is studied via potential stepping in both negative and positive directions (ND and PD), probably due to still ongoing reduction processes of the material itself.

We wondered if changes to the electrolyte over time were influencing the observed behaviors. Replacing the electrolyte with fresh solution and re-testing at −0.7 V results in reproducible product distributions with high FE_{HCOO^-}. This indicates that the prominent $HCOO^-$ selectivity is not arising solely from changes to the original electrolyte resulting from the electrochemical activation procedure (e.g., dissolved sulfur accumulation).

From all electrocatalytic activity experiments up to now, it can be generally concluded that behaviors are very dependent on the sequence of tests (stepping between potentials and performing linear sweep voltammetry-LSV-beforehand), with overall trend suggesting that electrodes activated at –0.9 V enhance $HCOO^-$ production and accordingly suppress the HER. As it is known that Cu sulfides become progressively reduced during cathodic operation, we next sought to identify the conditions leading to sulfur loss, quantify the post-electrolysis sulfur in the electrolyte and electrode and finally identify and quantify the Cu and S speciation under quasi in situ conditions.

2.3. In Situ EC-MS Tracking of Gaseous Sulfur Loss, Quantification of Residual Sulfur in the Electrocatalysts and Additional Experiments

The gas outflow of the electrochemical cell was sampled by capillary inlet mass spectrometer (MS) to identify volatile species evolved via reduction of Cu_xS under CO_2 electrolysis conditions. We found that H_2S (m/z signals 33 and 34) starts to evolve at potentials ≈–0.47 V during the first LSV scan (see **Figures 3** and S26, Supporting Information). The reduction of the Cu_xS generates S^{2-} (Equation 2) which is in equilibrium with HS^-/H_2S[44,51] (Equations 3 and 4) under near neutral pH.

$$Cu_xS\,(s) + 2e^- \rightarrow xCu^0\,(s) + S^{2-}\,(aq)\quad E_{Onset} = -0.47\ V\ versus\ RHE \tag{2}$$

$$S^{2-}\,(aq) + H^+\,(aq) \rightleftharpoons HS^-\,(aq) \tag{3}$$

$$HS^-\,(aq) + H^+\,(aq) \rightleftharpoons H_2S\,(aq) \rightleftharpoons H_2S\,(g) \tag{4}$$

Higher applied overpotentials resulting in higher currents typically leads to shorter H_2S evolution duration which indicates higher H_2S production rate (Figure 3). Namely, the H_2S evolution rate reaches a maximum at –0.9 V during the first LSV scan, decreases during the second and third scan and flattens ≈17 min after this potential is applied under stepped-potential mode (referred as "electrochemical activation" in the previous sections), as presented in Figure 3a. On the other hand, when the LSV scans are performed from 0 to –0.5 V, then the applied potential is stepped in negative direction starting from –0.5 V, Cu_xS needs more time to reduce leading to evolution duration of ≈1 h (Figure 3b) due to the lower current. For comparison, no m/z signals of 33 and 34 are observed from pristine Cu foam examined in the same manner, showing that these signals originate from H_2S generated by reduction of Cu_xS (Figure S26c, Supporting Information).

Examining the j–E behaviors during repeated cathodic LSV scans (Figure S27, Supporting Information), the initial scan shows two distinctive reduction features, the first a sharp wave at ≈–0.27 V and the second a broader one starting at –0.55 V continuing to –0.75 V. By comparing to the behavior of bare Cu foam (Figure S27c, Supporting Information), we believe that the first wave likely originates from reduction of residual native Cu-oxides present in the Cu_xS foam, in agreement with the Pourbaix diagram for the Cu-H_2O system,[52] which predicts the oxide phase can be reduced ≈–0.2 V under neutral pH.[53] The second, broad reduction feature we attribute to reduction of the Cu_xS in accordance with reports in the literature,[24,29,42,44] and its complex peak shape likely arises from the mixed-phase Cu:S composition.[54] The second and third LSV scans for the Cu_xS foam do not show any typical features suggesting that thorough reduction of the Cu_xS already completed during the first LSV scan.

In both direction of stepping the applied potential, there is no more observable H_2S evolution at –0.7 V where peak $HCOO^-$ selectivity is observed (Figure 2a,b) and from a thermodynamic point of view, Cu_xS should be completely reduced to metallic Cu at all potentials more negative than –0.7 V under near neutral pH.[22,24,29,42,44] Yet, according to various reports in the literature, this reduction is kinetically sluggish thus sulfur residues may persist during and after the electrolysis.[21,24,28,29,42] Therefore, we next sought to examine whether there is any significant difference in the electrocatalyst's bulk sulfur content that could relate the initial electrochemical activation with the $HCOO^-$ selectivity enhancement.

The bulk composition analysis of the Cu_xS foam with EDX shows that the sulfur content resembles ≈30 at.% for the as-prepared material and drops to ≈1 at.% following electrolysis at all applied potentials except at –0.5 and –0.6 V (≈1.5 at.%) when the potential is stepped in ND (Figure S28, Supporting Information). Additionally, XRD analysis for the Cu_xS foam post-electrolysis shows no peaks attributable to sulfide phases (see Figure S6, Supporting Information). Similar low sulfur content was reported in the literature for the best producing $HCOO^-$ electrocatalysts derived from Cu_xS.[29,43,44]

It can be presumed that certain amount of $S^{2-}/HS^-/H_2S$ species in equilibrium remains dissolved in the electrolyte for certain amount of time, possibly with different concentration dependent on the applied potential or "electrochemical activation" that affects the product selectivity. To test this hypothesis,

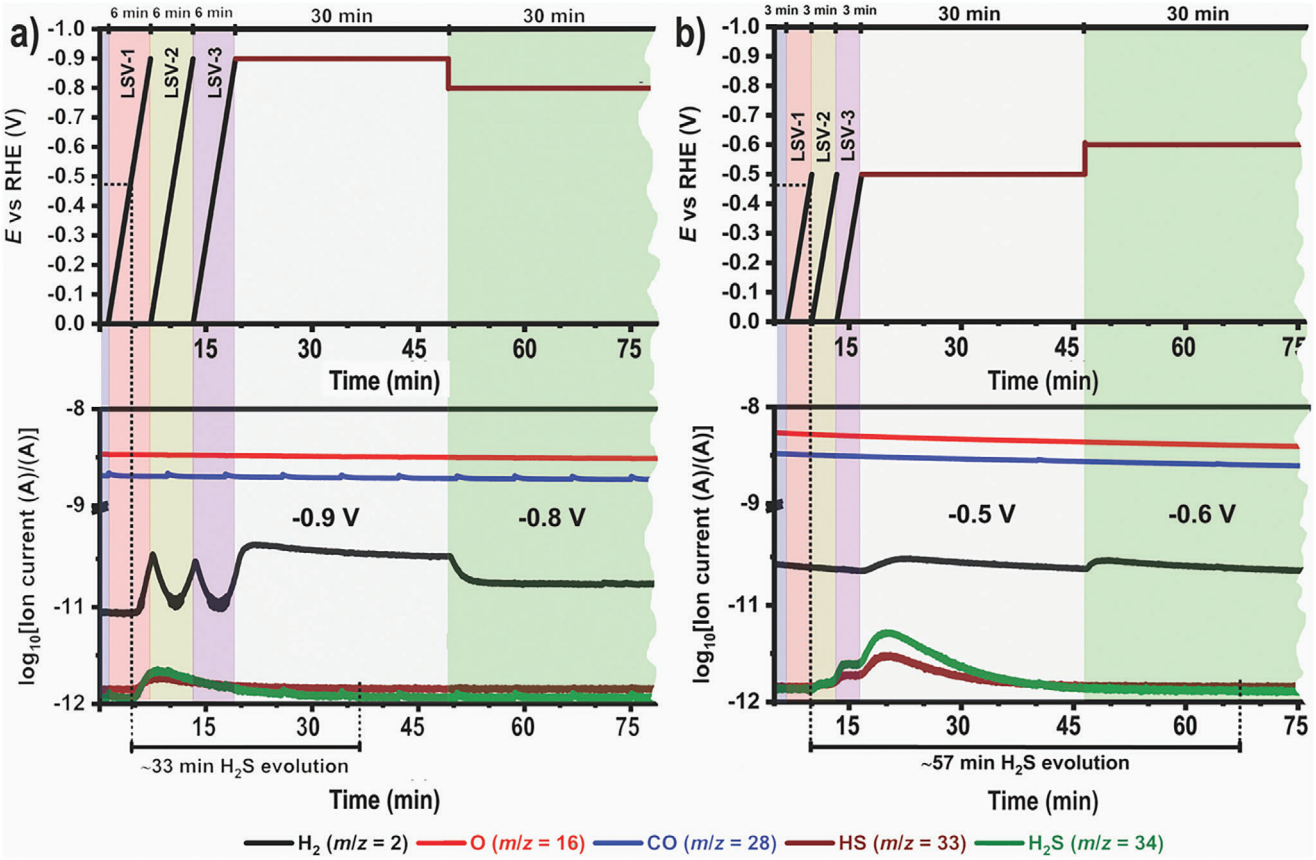

Figure 3. In situ electrochemical mass spectrometry (EC-MS) tracking of product evolution during scanning with linear sweep voltammetry – LSV and stepping the applied potential on Cu_xS foam electrodes in CO_2 saturated $KHCO_3$ (aq): a) 3 x LSV (0 to –0.9 V) and stepping in positive direction – PD (–0.9 to –0.5 V) and b) 3 x LSV (0 to –0.5 V) and stepping in negative direction – ND (–0.5 to –0.9 V). Mass/charge – *m*/*z* signals of 2, 16 and 28 are attributed to H_2, O_2 and CO, respectively and the *m*/*z* of 33 and 34 are attributed to H_2S. Shown here are the first two steps of the potential stepping; the full potential range data is presented in Figure S26 (Supporting Information).

pristine Cu foam samples were immersed in electrolytes in which previously Cu_xS foam was electrochemically reduced to produce dissolved sulfur species using one LSV scan from 0 to –0.9, –0.5 or to –0.7 V (referred as Cu+S foam electrode) and then their CO_2EC activity was examined at –0.9 and –0.7 V. Some literature reports have shown that electrolyte containing S^{2-} or purged with CO_2 containing small amounts of H_2S or SO_2 can result in formation of $HCOO^-$ selective Cu_xS electrocatalysts.[21,22,27,32]

The electrocatalytic activity results obtained on the Cu+S foam electrodes are presented in **Figure 4** and as replotted and extended version in Figure S29 (Supporting Information), while the experimental conditions and sample abbreviations are explained in Table S1 (Supporting Information).

When a pristine Cu foam is tested in electrolyte which was previously used for a single LSV scan of a Cu_xS foam electrode to either –0.9 or –0.7 V (resulting samples: Cu+S foam-0.9 and Cu+S foam-0.7), the $HCOO^-$ production is significantly enhanced compared to pristine Cu foam. Comparing these results with Cu_xS foams-PD/ND at –0.9 V, the Cu+S foam-0.9/-0.7 electrodes show higher FE_{HCOO^-}. On the other hand, when Cu foam is tested using electrolyte in which Cu_xS foam was reduced to –0.5 V again with a single LSV scan (sample: Cu+S foam-0.5), the FE_{HCOO^-} is significantly lower, compared to the Cu+S foam samples prepared via reducing the Cu_xS foam with LSV to –0.9 or –0.7 V. The lower $HCOO^-$ selectivity in the case of Cu+S foam-0.5 sample suggests that perhaps the amount of electrolyte sulfur species obtained with one LSV reduction of the Cu_xS foam is selectivity-wise not sufficient since the potential of –0.5 V is near the onset potential for Cu_xS reduction (Equation 2).

The selectivity results obtained on Cu+S foam electrodes that were examined at –0.7 V (after electrochemical activation at –0.9 V), did not show drastic differences in FE_{HCOO^-} when compared to Cu_xS foam-PD (Figure S29, Supporting Information).

Repeating the same experiment in which Cu+S foam electrodes (detailed description in Table S1, Supporting Information) were prepared via immersing Cu foam in electrolyte under various conditions (1 h of continuous CO_2 purging prior to applying bias – electrode annotated as Cu+S foam-P1 h, immersing in electrolyte without CO_2 purging prior to electrolysis, annotated as Cu foam-S-NP and Cu+S foam-P1 h electrode prepared in electrolyte with sulfur species but tested in fresh electrolyte – annotated as Cu+S foam-P1h-NE), no significant difference in the FE_{HCOO^-} can be observed at –0.7 and at –0.9 V, when compared to all samples prepared via LSV reduction from 0 to –0.9 V (Figure S29, Supporting Information).

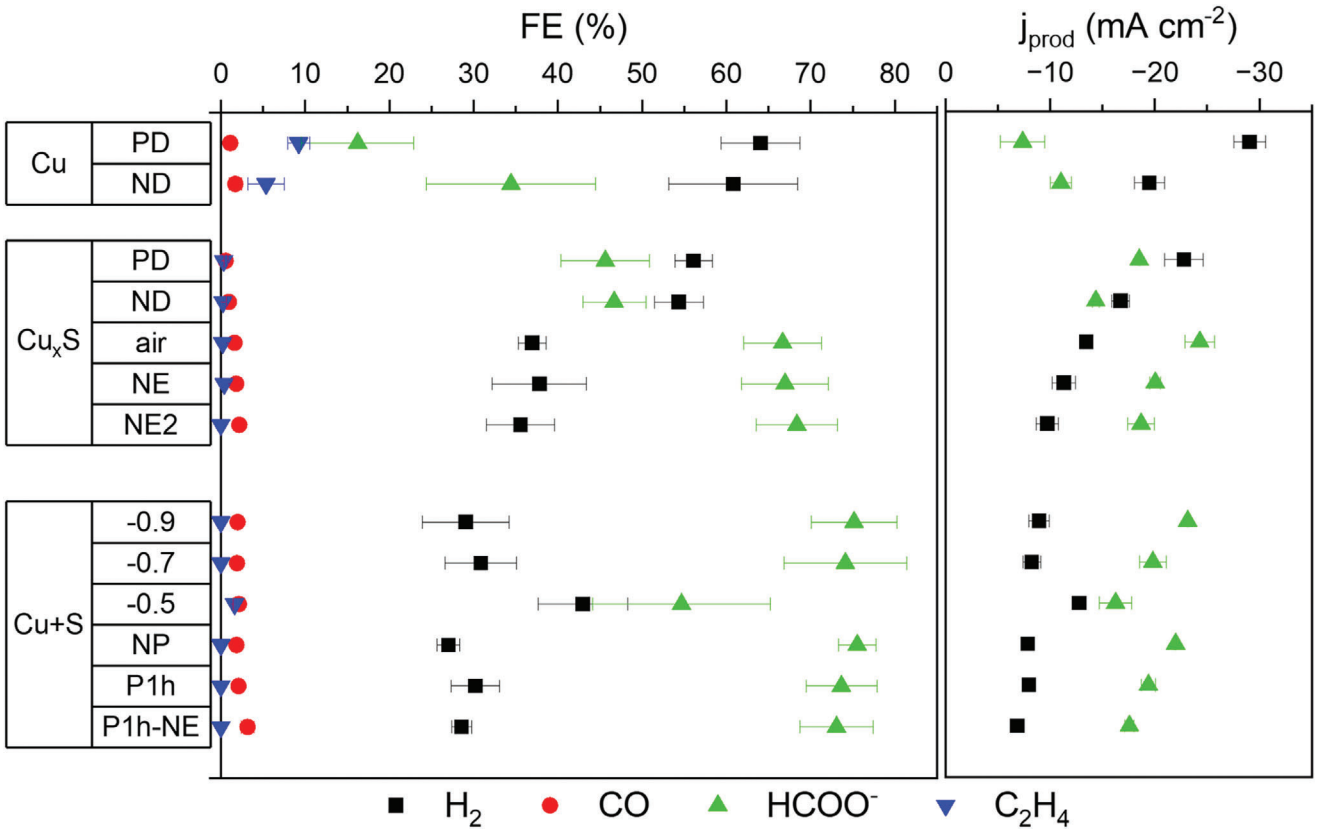

Figure 4. Distribution of FE for H_2 and CO_2EC products and partial current densities for H_2 and $HCOO^-$ obtained on Cu_xS foam and Cu+S foam under 1 h electrolysis at applied potential of –0.9 V after "electrochemical activation".

Regarding the surface morphology, the Cu+S foam electrodes dendrite microstructures, examined post-electrolysis did not transform into sponge-like features but rather preserve the dendrite microstructures as in pristine Cu foam (Figures S30 and S31, Supporting Information). This is suggesting that most probably the selectivity is not affected by the surface morphology.

Additionally, several other experiments were conducted in which already examined Cu_xS foam-PD samples (activated at –0.9 V) were re-examined at the same potentials after being exposed to air, or the electrolyte was replaced once or two times (abbreviated as: Cu_xS foam-air, Cu_xS foam-NE and Cu_xS foam-NE2, respectively). The results in Figures 4 and S29 (Supporting Information) show $HCOO^-$ selectivity enhancement at –0.9 V, while somewhat lower FE_{HCOO^-} for Cu_xS foam-air and similar for Cu_xS foam-NE and Cu_xS foam-NE2 at –0.7 V, when compared to Cu_xS foam-PD.

These findings could give a presumption that the selectivity may be affected by electrodes surface composition and concentration of dissolved sulfur species in the electrolyte that are possibly related to the initial electrochemical activation at –0.9 V. Therefore, for further clarification, the surface composition and electrolyte dissolved sulfur obtained from reduction of Cu_xS foam were studied under various experimental conditions with quasi in situ XPS and ICP-OES, respectively and the results are discussed and summarized in the following section.

Acronyms: PD: positive, ND: negative direction (of stepping the applied potential), air: refers to electrode exposed to air and retested; NE/NE2: new electrolyte and new electrolyte placed second time (retesting electrodes in fresh electrolyte); Cu+S: refers to electrodes obtained by placing Cu foam in electrolyte in which Cu_xS foam was previously reduced; NP: not purged/P: purged with CO_2 for 1 h (while Cu foam stays in the cell); P1h-NE: Cu_xS electrode prepared in electrolyte with sulfur species but tested in fresh (new) electrolyte. The full list of sample abbreviations and experimental conditions are presented in Table S1 (Supporting Information) and the data from all tested samples in Figure S29 (Supporting Information).

2.4. Quantification and Speciation of the Surface Cu and S, Analysis of the Electrolyte Sulfur and Overall Summary of the Composition-Structure-Activity Relations

Seeking for answers whether the electrochemical activation of the electrocatalysts that causes $HCOO^-$ selectivity enhancement is somehow related to surface changes in terms of Cu:S composition and oxidation states (speciation), we examined the materials with quasi in situ XPS. As already known from the literature[21,24,28,29,33,42] and supported in this study from the EDX analysis that sulfur species do persist during the CO_2 electrolysis, to the best of our knowledge the chemical nature related to speciation and oxidation state of Cu and S under operating or near-operating conditions are not yet resolved. Due to sulfur's low molecular mass and low-energy x-ray transitions, in situ x-ray

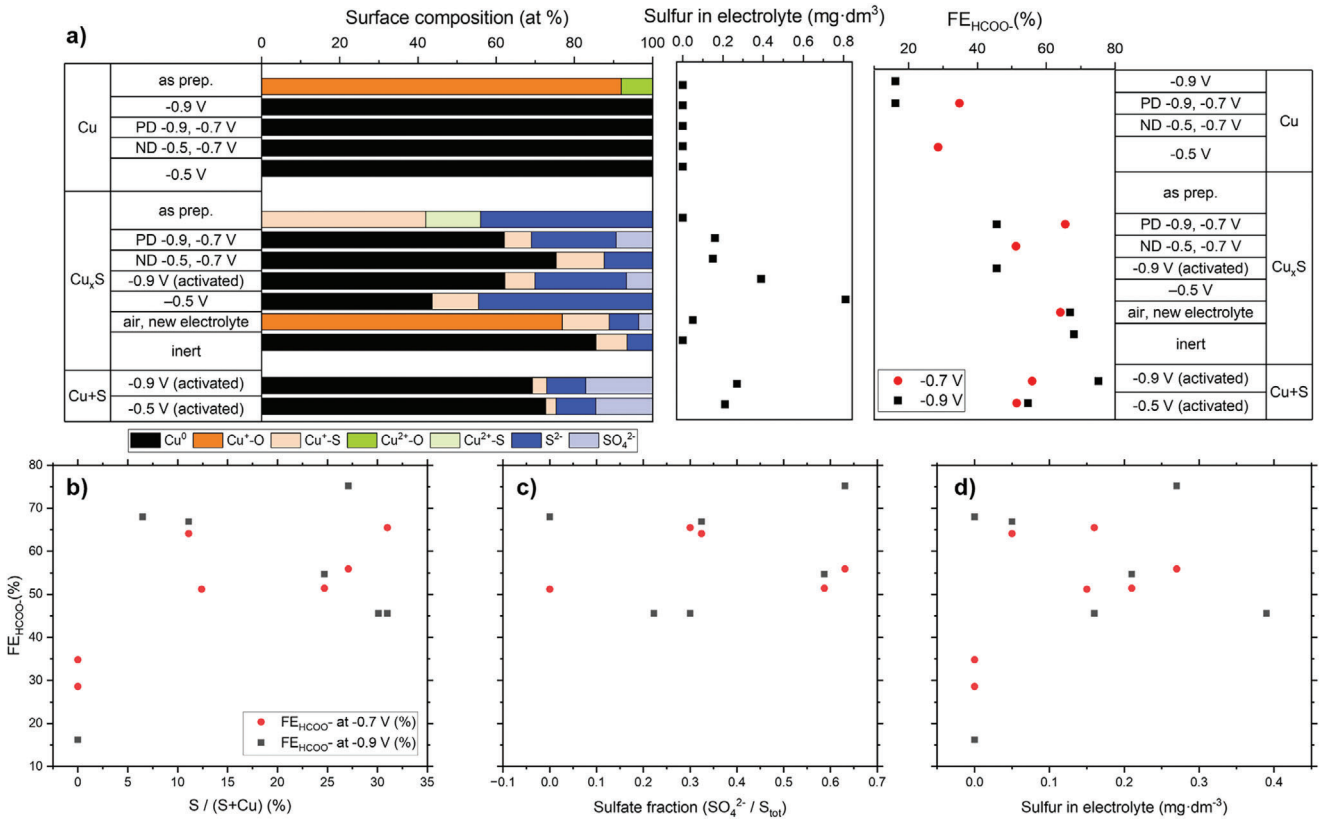

Figure 5. Overall summary showing relations between electrode surface composition, electrolyte sulfur species and FE for CO_2 to $HCOO^-$ conversion: a) Electrode surface composition, dissolved sulfur content, and FE for $HCOO^-$ for the various catalysts and testing conditions. The FE $HCOO^-$ activity for each sample is re-plotted versus various possible descriptors: b) catalyst total sulfur fraction, c) catalyst sulfate fraction, and d) quantity of dissolved sulfur species in electrolyte. All data is presented in Table S4 (Supporting Information).

absorption spectroscopy measurements of sulfur are extremely challenging. Therefore, XPS was used to study the electrode surfaces, using the quasi in situ approach in which electrochemical testing (N_2 filled glovebox) and sample transfer into the XPS analyzer was maintained under inert environment to prevent air-induced re-oxidation. ICP-OES was used to quantify dissolved sulfur in the electrolyte following electrochemical experiments. Experimental details for these methods are provided in Section S1.5. (Supporting Information).

The XPS survey spectra for all samples are presented in Figure S34 (Supporting Information) and the Cu 2p, O 1s, Cu LMM Auger and S 2p spectra are presented in Figures S35–S38 (Supporting Information). The Cu 2p core level XPS spectra in Figure S35 (Supporting Information) show that the surface Cu species resemble either metallic (Cu^0) or Cu^+ oxidation state from the Cu $2p_{3/2}$ peak positions at ≈932.5 eV in the case of all examined materials, except for pristine Cu and Cu_xS where additional peaks at ≈934 eV corresponding Cu^{2+} can be observed.[55] This is expected since the surface of the as-prepared Cu foam is prone to oxidation in air. The Cu 2p in the as-prepared Cu_xS foam resembles mixed Cu^+/Cu^{2+} species. The lattice oxygen species at ≈530.5 eV attributed to O 1s[55] in the catalysts surface structure can be only observed in the air exposed samples but not in the ones subjected to the electrolysis under inert conditions, as presented in Figure S36 (Supporting Information).

Cu LMM Auger spectra was used for speciating the Cu oxidation states since it better discriminates the oxidation states and chemical environments of Cu, compared to Cu 2p spectra. The Cu Auger spectra are presented in Figure S37 (Supporting Information) and the extracted results regarding speciation and quantification of the electrocatalysts surface, in Table S4 (Supporting Information) and **Figure 5**a. Those results show that the pristine Cu foam resembles dominant Cu^+ and small fraction of Cu^{2+} originating from Cu_2O and CuO, respectively. The presence of oxidized Cu species on the surface of this material supports the above mentioned Cu^{2+} assigned peaks in the Cu 2p spectra and the lattice oxygen species signal in the O 1s XPS spectra. The presence of Cu_2O as main surface phase agrees with the XRD data for this material (Figures 1c and S6, Supporting Information). Considering the Cu_xS foam, the surface is composed of ≈75 at.% Cu^+ and ≈25 at.% Cu^{2+} originating from Cu_2S and CuS, respectively. When negative electrochemical bias is applied, the pristine Cu foam undergoes complete surface reduction to metallic Cu in the case of all examined samples regardless of the potential and direction in which it is applied in the range between −0.5 and −0.9 V. This is in agreement with our previous publication's XPS results showing that under reductive bias under similar range of applied potentials, the Cu foam's surface resembles only metallic Cu.[47]

On the other hand, the Cu Auger spectra results show that during the reduction process, the Cu_xS foam undergoes significant but incomplete reduction to metallic Cu, with 10–15 at.% Cu^+ associated to Cu_2S observed at applied potential of −0.9 V (activation) and also at −0.7 V when the potential is stepped in positive (PD, −0.9 to −0.7 V) and in negative (ND, −0.5 to −0.7 V) direction. However, at −0.5 V, the fraction of Cu^+ associated with Cu_2S is higher (≈22 at.%) which, as stated in the previous sections is expected, considering that the reduction of the material is sluggish at this potential since it is near the onset potential for this process (Figure S27, Supporting Information) and higher bulk sulfur amount in the catalyst is observed (≈1.5 at.% from EDX – Figure S28, Supporting Information). It seems that the initial activation of the Cu_xS foam electrocatalyst cannot be only explained from the Cu^+ fractions which are not significantly different at −0.7 V, regardless of the potential stepping direction. Regarding the Cu_xS foam that was exposed to air after electrolysis and re-examined in a fresh electrolyte at −0.9 and −0.7 V and then analyzed ex situ, showed fully oxidized surface without any presence of metallic Cu (Figure 5a). This material contains ≈13 at.% Cu^+ associated to Cu_2S, similar as in the case of Cu_xS foam examined via stepping the potential in positive – PD (−0.9 and −0.7 V) and negative – ND (−0.5 and −0.7 V) direction, but however, the remaining ≈87 at.% are attributed to Cu^+ associated to Cu_2O. Contrary to this, when Cu_xS foam is examined via the same manner but under inert (N_2 filled glovebox) conditions, no evidence of Cu^+ originating from Cu_2O is observable and the surface consists of metallic Cu and ≈8 at.% Cu^+ from Cu_2S, that is not much different than the air exposed one.

The Cu+S foam electrocatalysts prepared via immersing Cu foam in electrolyte in which Cu_xS foam electrode was previously reduced with one LSV scan to −0.5 and −0.9 V (Cu+S foam-0.5 and Cu+S foam-0.9), besides metallic Cu as main surface fraction, contain 3–5 at.% Cu^+ species attributed to Cu_2S. The surfaces of both materials have similar Cu^+ fraction, but at −0.9 V much higher $HCOO^-$ selectivity is observed in the case of Cu+S foam-0.9 (see Figure 4a).

Figure 5a also shows the quantification results for sulfur species obtained from the S 2p core levels (assigned to S^{2-} at ≈162 eV and SO_4^{2-} at ≈170 eV[21,56] – Figure S38, Supporting Information). Besides S^{2-}, the existence of SO_4^{2-} specie is unusual considering that the sulfur in SO_4^{2-} is in its highest oxidation state (+6) and it appears on the surface of a cathode material. Contrary to what was observed from the EDX results in Figure S28 (Supporting Information) where the bulk sulfur fraction at −0.7 V is not much different regardless of the potential stepping direction, the surface sulfur speciation and fraction do show some differences. Specifically, at −0.7 V, where in dependence from the potential stepping sequence, higher FE_{HCOO^-} is observed when stepped in positive direction – PD (from −0.9 to −0.7 V), i.e., activated, the Cu_xS foam resembles higher S^{2-} and total sulfur fraction compared to the case when the potential is stepped in negative direction – ND starting from −0.5 V. This is the first observation showing evident differences in the catalyst composition caused by the electrochemical activation.

However, significantly lower total sulfur and S^{2-} are observed in the case of Cu_xS foam-NE (re-examined in fresh electrolyte) which shows identical FE_{HCOO^-} at −0.7, while higher at −0.9 V compared to Cu_xS foam-PD (stepped in positive direction – PD, i.e., activated). Nevertheless, the Cu+S foam-0.9/-0.5 samples show almost identical total sulfur and S^{2-} fractions but their electrocatalytic performance differs in terms of achieving higher FE_{HCOO^-} on Cu+S foam-0.9, especially at −0.9 V. Comparing the Cu+S foam-0.9 with Cu_xS foam-PD, the FE_{HCOO^-} is significantly higher at −0.9 V and lower at −0.7 V in the case of Cu+S foam-0.9, while both materials show similar total sulfur but higher S^{2-} fraction. Therefore, only the total surface sulfur and/or the S^{2-} fractions can hardly corelate with the $HCOO^-$ selectivity in a general case, but this will be further discussed later in the text when the electrolyte dissolved sulfur is taken into consideration.

Regarding the identification of surface SO_4^{2-}, the presence of this specie is observed in all Cu_xS foam samples subjected, i.e., activated at −0.9, but not when the electrolysis is conducted at −0.5 V or the potential is stepped from −0.5 to −0.7 V (negative direction – ND) as showed in Figures 5a and S38 (Supporting Information). In the latter case, the sulfur exclusively resembles S^{2-}. However, in the case of the sample exposed to inert atmosphere SO_4^{2-} cannot be fitted and fully identified due to the noisiness of the spectrum but cannot be fully excluded. The formation of SO_4^{2-} must occur via oxidation of S^{2-} since there is no other sulfur source but it is rather not evident why this is observable only when potential of −0.9 V is applied. Surface SO_4^{2-} detected with ex situ XPS, is already reported in the literature for Cu nanoparticles that were sulfidated with SO_2 during electrolysis at potentials similar or more negative compared to our case (−0.9 V).[21] They suggest natural oxidation of metal sulfides which is rather different than our case since the electrolysis for the samples subjected to XPS analysis was performed under inert conditions. A possible explanation is that the SO_4^{2-} specie results from chemical oxidation of dissolved S^{2-} triggered by the strong alkaline environment[57] which results near the cathode during CO_2EC, with local pH increase proportional to the current density.[58] Therefore, it is expected that the oxidation of S^{2-} into SO_4^{2-} occurs locally in the electrolyte near the electrode surface thus SO_4^{2-} is observed on the surface of the electrocatalyst. In analogy to these findings, malachite and azurite phases where Cu is in oxidation state +2 were found with in situ Raman spectroscopy under operating electrolysis at reductive bias on bare Cu foam, while the quasi in situ XPS results showed presence of only metallic Cu, as reported in our previous study.[47]

In the following text, the discussion will be focused on summarizing the findings and relating the catalysts surface composition and electrolyte dissolved sulfur species with the activity for CO_2 to $HCOO^-$ conversion. An overall schematic of this study is presented in Scheme S1 (Supporting Information).

Observing the results in Figure 5a, it is obvious that the as-prepared Cu_xS foam undergoes significant surface sulfur loss in all cases except at −0.5 V when the total surface sulfur fraction is similar as in the case of the as-prepared material due to lower current. Nevertheless, under reduction at −0.5 V the concentration of dissolved sulfur is the highest and moreover the dissolved sulfur species retain the longest in the electrolyte (under lower current), compared to all other cases. This behavior agrees with the results in Figure 3b (longer H_2S evolution duration). Even though, as already discussed previously in the text, there is a difference in the surface sulfur fractions on the basis of the potential stepping sequence (referring to the activation effect) when higher surface sulfur was observed in the case of the Cu_xS foam

at −0.7 V previously activated at −0.9 V (showing higher FE_{HCOO^-} at −0.7 V in comparison when stepping in negative direction – ND), there is no big difference in the concentrations of dissolved sulfur (Figure 5a).

Somewhat similar dissolved sulfur concentrations and also not significantly different total sulfur fraction is observed post-electrolysis for the Cu+S foam-0.9/-0.5 electrodes compared among each other, even though there are discrepancies in the $HCOO^-$ selectivity, especially at −0.9 V. When the Cu+S foam-0.9/-0.5 are compared to the Cu_xS foam-PD/ND electrodes, there is not much difference in the concentration of electrolyte dissolved sulfur in all cases and also for the surface sulfur fractions for the Cu_xS foam-PD and Cu+S foam-0.9/-0.5, but however it is difficult to observe clear correlation with the FE_{HCOO^-}, which shows the highest values for Cu+S foam-0.9 at −0.9 V, whilst for Cu_xS foam-PD when examined at −0.7 V.

Finally, the catalyst examined after replacing the electrolyte – Cu_xS foam-NE (NE – new electrolyte) show almost similar FE_{HCOO^-} with Cu+S foam-0.9 when examined at –0.9 V, but higher for Cu_xS foam-NE at –0.7 V (Figures 5 and S29, Supporting Information), and the electrolyte dissolved, and surface sulfur contents are smaller for the samples examined after placing new electrolyte. Moreover, when comparing the Cu_xS foam-NE (re-examined in fresh electrolyte) and Cu_xS foam-inert (re-examined in fresh electrolyte but the electrolyte was replaced under inert conditions and the sample was not exposed to air), there is no difference in FE_{HCOO^-} at –0.9 V and also not much difference in the S^{2-} fraction and which is suggesting that air oxygen exposure during sample handling does not per se affects the selectivity.

Having a look at the graphs in Figure 5b–d plotting the electrode surface composition and electrolyte sulfur species versus the FE for CO_2 to $HCOO^-$ conversion, it is rather hard to make a straightforward relation between catalyst and electrolyte sulfur composition versus the $HCOO^-$ selectivity, and this is because the surface versus electrolyte sulfur distribution could be very dynamic considering Cu_xS reductive dissolution (Equation 5) and dissolved sulfur redeposition (Equations 6 and 7) when metallic Cu reacts with dissolved H_2S and S^{2-} having in mind the scattering of the S^{2-} surface fraction and electrolyte dissolved sulfur species while reaching similar values for FE_{HCOO^-}. The reaction between Cu and dissolved sulfur species (such as S^{2-}) is a well-known phenomenon, additionally a recent report claims that such species can progressively penetrate into Cu's surface.[32]

$$Cu_xS\,(s) + 2H^+\,(aq) + 2e^- \rightarrow xCu^0\,(s) + H_2S\,(aq) \quad (5)$$

$$xCu^0\,(s) + S^{2-}\,(aq) \rightarrow Cu_xS\,(s) + 2e^- \quad (6)$$

$$xCu^0\,(s) + H_2S\,(aq) \rightarrow Cu_xS\,(s) + 2H^+ + 2e^- \quad (7)$$

It somehow appears that the electrochemical activation at high overpotential provides faster removal of the excess sulfur from the catalyst surface due to higher passed charge leading to higher $HCOO^-$ selectivity when comparing Cu_xS foam-PD versus ND at −0.7 which further enhances but only significantly at −0.9 V when either the electrolyte is replaced with a fresh one or pristine Cu foam is placed in electrolyte with dissolved sulfur species (which can be considered as further decrease of excess sulfur). In all cases the concentration of electrolyte dissolved sulfur should be ≤0.3 mg·dm^{-3} and surface sulfur fraction ≤30 at.% in order to achieve at least 50% FE_{HCOO^-}.

From a mechanistic point of view, and as discussed in the introduction, it is generally proposed in the literature,[21,23,26,29,31,33,59] that CO_2 selectively converts into $HCOO^-$ via the *OCHO* intermediate (also referred as OCHO* or HCOO*) which prefers oxophilic binding on partially positive Cu species on Cu_xS catalyst's surface. Moreover, the presence of sulfur in Cu's structure inhibits the binding of H* – responsible for HER[26,33] and of *CO[26,59] or *COOH[29,59] which can desorb as CO or further reduce into C_{2+} products via multielectron steps. The schematic representation of the mechanism proposing a CO_2 transformation into Cu^+ (which is empirically determined in this research) bound *OCHO* intermediate via single proton-coupled-electron transfer and subsequent formation of $HCOO^-$ in a second electron step, is presented in Scheme S1 (Supporting Information). The mechanistic studies reported in the literature, that are supporting the CO_2 to $HCOO^-$ conversion pathways via the *OCHO*/OCHO*/HCOO* intermediate, are generally obtained from in situ Raman and in situ ATR-IR spectroscopy and/or theoretically predicted using DFT calculations.

A final observation is that the presence of SO_4^{2-} species on the surface of the electrocatalyst is in relation with the electrochemical activation at −0.9 V that leads to enhanced $HCOO^-$ production, but it cannot be claimed that the SO_4^{2-} is the direct reason for this activity enhancement. Regarding the relation between the selectivity and the actual fraction of this specie, even though the highest FE_{HCOO^-} at −0.9 V corresponds to the highest SO_4^{2-} fraction (in total sulfur, Figure 5c), it is rather difficult to draw conclusions due to the higher solubility of SO_4^{2-} compared to S^{2-} and the aforementioned dynamicity of the electrode-electrolyte sulfur distribution. This can cause uncertainties for proper quantification of total sulfur and probably SO_4^{2-} causing uncertainty whether this specie is incorporated into the structure of the electrocatalyst material, or it is only a surface deposit. If SO_4^{2-} are incorporated into Cu_xS structure and affect the electronic properties of Cu, it could be possible that this specie participates in the stabilization of Cu^+, as presented in Scheme S1 (Supporting Information).

Characterization of the electrocatalyst under in situ conditions with near ambient XPS and soft x-ray absorption spectroscopy (XAS) under running electrolysis is worth considering for a future study. Moreover, estimation of the local pH change with in situ Raman or IR spectroscopy and possible quantification and speciation of the electrode-electrolyte interface sulfur could provide more evidence for better understanding of how the electrochemical activation enhances the $HCOO^-$ selectivity and how the SO_4^{2-} specie is formed under reductive bias.

3. Conclusion

- In this study, a facile method combining electrochemical DHBT deposition of Cu foam with subsequent chemical sulfidation using sulfur saturated toluene solution was developed for synthesis of Cu_xS foam electrocatalyst for CO_2 conversion into $HCOO^-$.
- It was found that the as-prepared Cu_xS resembles mixed phase composition from digenite and roxbyite with nominal

stoichiometry of $Cu_{1.8}S$ and foam morphology composed of dendrite microstructures.

- The results from the electrocatalytic activity showed that on Cu_xS foam, CO_2 converts almost exclusively to $HCOO^-$ and simultaneously HER is suppressed, compared to pristine Cu foam.
- Cu_xS foam electrodes underwent reduction accompanied by morphological transformation from dendrite into sponge-like microstructures, leading to significant loss of sulfur as H_2S and dissolved sulfur species.
- The reduction of Cu_xS foam is not complete even at potentials as negative as –0.9 V, that is, besides metallic Cu, partially oxidized copper (Cu^+) and residual sulfur species are observed, while the surface of pristine Cu foam fully transforms into Cu^0 at all tested potentials. This implies that the sulfur species are stabilizing the Cu^+ sites on the electrocatalyst surface in correlation with enhancement of the CO_2 to $HCOO^-$ conversion selectivity compared to pristine Cu foam.
- It was found that the $HCOO^-$ selectivity depends on the applied potential value as well as the potential testing sequence. Higher $HCOO^-$ selectivity is observed at –0.7 V when the potential is first activated at –0.9 V compared to when it is increased progressively from low to high overpotential.
- Regardless of the Cu_xS foam preparation and treatment, no obvious trends directly correlating the $HCOO^-$ selectivity with various possible descriptors (measured surface fraction of Cu^+/S^{2-}, dissolved sulfur species) were observed, indicating dynamic electrode-electrolyte sulfur distribution that is difficult to capture via ex situ measurements. However, it can be claimed that total surface sulfur fraction ≲30 at.% and concentration of electrolyte dissolved sulfur ≲0.3 mg·dm^{-3} are required to achieve min 50% FE_{HCOO-} at both –0.9 and –0.7 V.
- Besides S^{2-}, spectroscopic evidence suggests SO_4^{2-} forms when the electrodes are subjected to applied potential of –0.9 V, again indicating dynamic local environment effects leading to formation of this specie under higher overpotentials, which may also contribute to stabilization of Cu^+. The SO_4^{2-} specie can be considered an empirical descriptor correlating with the electrochemical activation of the Cu_xS catalysts and therefore further study of the electrochemical interface under in situ conditions is worth pursuing for better understanding of these effects.

4. Experimental Section

All reagents and materials utilized for this study are listed and described in Section S1.1. (Supporting Information). The synthesis of sulfidated Cu_xS foam electrodes was accomplished by a sequence of several brief steps. In the first step, dendritic Cu foam was electrodeposited under dynamic H_2 bubble template (DHBT)[47] conditions on pre-cleaned Cu mesh cathode in an aqueous solution of 0.2 mol·dm^{-3} $CuSO_4$ and 1.5 mol·dm^{-3} H_2SO_4, by applying current density of –5 A•cm^{-2} (relative to geometric area) for a duration of 9.5 s. A two-electrode setup with Cu foil as an anode was used for this purpose. The schematic for the materials preparation, electrodeposition procedure and setup are depicted in Figure S1 (Supporting Information) and all information regarding the electrochemical processes during the DHBT deposition are presented and discussed in Section S1.2 (Supporting Information). In a following step, the as-prepared Cu foam was sulfidated by immersing the samples in room temperature sulfur-saturated toluene solution for 3 s. The materials, chemicals and detailed experimental procedures are described in Section S1.3. (Supporting Information) and presented in Figure S2 (Supporting Information).

The chemical and phase composition of the materials were characterized with x-ray diffraction (XRD), energy dispersive x-ray (EDX) spectroscopy, in situ thermogravimetric analysis coupled with mass spectrometry (TGA-MS) and differential scanning calorimetry (DSC). The atomic fractions and oxidation states (speciation) of surface Cu, S and O were studied using x-ray photoelectron spectroscopy (XPS) under ex situ and quasi in situ approaches, where in the latter case the analyzer was coupled with transfer vessel in which samples were loaded directly from a glovebox where electrochemical experiments were conducted under inert environment. The surface morphology and pore sizes were evaluated using scanning electron microscopy (SEM). The thickness of the foams was determined from cross-section SEM after vertical ablation of the samples using focused ion beam (FIB).

Electrocatalytic activity measurements were conducted in H-type gas-flow cell filled with 0.1 mol·dm^{-3} $KHCO_3$(aq) as a supporting electrolyte, constantly purged with CO_2 in the cathodic compartment and providing bias in linear sweep voltammetry (LSV) and chronoamperometric (CA) modes. The CO_2EC gaseous products and H_2 from HER were quantified using on-line gas chromatography (GC). The volatile (alcohols) and non-volatile CO_2EC liquid products ($HCOO^-$) were quantified post-electrolysis using headspace gas chromatography (GC-HS) and high-performance liquid chromatography (HPLC), respectively. The H_2S evolution during the electrolysis was followed via in situ electrochemical mass spectrometry (EC-MS) and the content of the sulfur species in the electrolyte was analyzed post-electrolysis with inductively coupled plasma-optical emission spectroscopy (ICP-OES). The materials characterization, electrochemical and product quantification methods are described in detail in Sections S1.4 and S1.5 (Supporting Information) The supporting results are presented in Section S2 (Supporting Information). All sample abbreviations and experimental conditions under which they were examined are listed and described in Table S1 (Supporting Information).

Supporting Information

Supporting Information is available from the Wiley Online Library or from the author.

Acknowledgements

The authors acknowledge Max Rieckert, René Gunder, Christian Höhn, Uttam Gupta, Claudia Leistner, Mahboubeh Maleki and Ursula Michalczik for experimental support and useful suggestions. This work was funded by the Helmholtz Association's Initiative and Networking Fund via the Helmholtz Young Investigators Group award (VH-NG-1225). The ICP-OES measurements were performed in the SolarFuelsTestingFacility (SFTF) Lab of the Helmholtz Energy Materials Foundry (HEMF). Additional financial support came from the European Union Horizon 2020 research and innovation program project FlowPhotoChem (Grant Agreement No. 862453). The material presented and views expressed here are the responsibilities of the authors only; the funding agencies take no responsibility for any use made of the information set out.

Open access funding enabled and organized by Projekt DEAL.

Conflict of Interest

The authors declare no conflict of interest.

Data Availability Statement

The data that support the findings of this study are openly available in [Zenodo] at [https://doi.org/10.5281/zenodo.13354297], reference number [13354297].

Keywords

CO_2 electrolysis, composition-structure-activity relations, copper sulfides, Cu^+ species, residual sulfur

Received: August 21, 2024
Revised: October 5, 2024
Published online: October 25, 2024

[1] J. Wu, Y. Huang, W. Ye, Y. Li, *Adv. Sci.* **2017**, *4*, 1700194.
[2] H. Ritchie, M. Roser, Energy: Fossil Fuels. Published online at OurWorldinData.org, Retrieved from: https://ourworldindata.org/fossil-fuels (accessed: August 2024).
[3] S. Nitopi, E. Bertheussen, S. B. Scott, X. Liu, A. K. Engstfeld, S. Horch, B. Seger, I. E. L. Stephens, K. Chan, C. Hahn, J. K. Nørskov, T. F. Jaramillo, I. Chorkendorff, *Chem. Rev.* **2019**, *119*, 7610.
[4] P. De Luna, C. Hahn, D. Higgins, S. A. Jaffer, T. F. Jaramillo, E. H. Sargent, *Science* **2019**, *364*, eaav3506.
[5] M. Jouny, W. Luc, F. Jiao, *Ind. Eng. Chem. Res.* **2018**, *57*, 2165.
[6] A. Dutta, M. Rahaman, N. C. Luedi, M. Mohos, P. Broekmann, *ACS Catal.* **2016**, *6*, 3804.
[7] R. Kortlever, J. Shen, K. J. P. Schouten, F. Calle-Vallejo, M. T. M. Koper, *J. Phys. Chem. Lett.* **2015**, *6*, 4073.
[8] J. B. Greenblatt, D. J. Miller, J. W. Ager, F. A. Houle, I. D. Sharp, *Joule* **2018**, *2*, 381.
[9] J. Hietala, A. Vuori, P. Johnsson, I. Pollari, W. Reutemann, H. Kieczka, *Wiley-VCH Verlag GmbH & Co. KGaA* **2016**, 1, https://doi.org/10.1002/14356007.a12_013.pub3.
[10] L. Lan, W. Yang, J. Li, L. Zhang, Q. Fu, Q. Liao, *ACS Appl. Mater. Interfaces* **2020**, *12*, 27095.
[11] Z. Yang, F. E. Oropeza, K. H. L. Zhang, *APL Mater.* **2020**, *8*, 060901.
[12] C. E. Moore, E. L. Gyenge, *ChemSusChem* **2017**, *10*, 3512.
[13] M. Rahaman, K. Kiran, I. Zelocualtecatl Montiel, A. Dutta, P. Broekmann, *ACS Appl. Mater. Interfaces* **2021**, *13*, 35677.
[14] M. d. J. Gálvez-Vázquez, P. Moreno-García, H. Guo, Y. Hou, A. Dutta, S. R. Waldvogel, P. Broekmann, *ChemElectroChem* **2019**, *6*, 2324.
[15] M. Ren, H. Zheng, J. Lei, J. Zhang, X. Wang, B. I. Yakobson, Y. Yao, J. M. Tour, *ACS Appl. Mater. Interfaces* **2020**, *12*, 41223.
[16] Y. Chen, K. Chen, J. Fu, A. Yamaguchi, H. Li, H. Pan, J. Hu, M. Miyauchi, M. Liu, *Nano Mater. Sci.* **2020**, *2*, 235.
[17] Y. Hori, *Modern Aspects Electrochem.* **2008**, *42*, 89.
[18] M. Poliakoff, P. Licence, M. W. George, *Current Opinion in Green and Sustainable Chemistry* **2018**, *13*, 146.
[19] G. B. Haxel, J. B. Hedrick, G. J. Orris, U.S. Geological Survey Fact Sheet 087-02 https://pubs.usgs.gov/fs/2002/fs087-02/, (accessed: August 2024).
[20] Daily Metal Spot Prices. Daily Metal Prices, https://www.dailymetalprice.com/metalpricescurr.php?x=USD (accessed: August 2024).
[21] W. Luc, B. H. Ko, S. Kattel, S. Li, D. Su, J. G. Chen, F. Jiao, *J. Am. Chem. Soc.* **2019**, *141*, 9902.
[22] J. W. Lim, W. J. Dong, J. Y. Park, D. M. Hong, J.-L. Lee, *ACS Appl. Mater. Interfaces* **2020**, *12*, 22891.
[23] Z. Pan, K. Wang, K. Ye, Y. Wang, H.-Y. Su, B. Hu, J. Xiao, T. Yu, Y. Wang, S. Song, *ACS Catal.* **2020**, *10*, 3871.
[24] D. Liu, Y. Liu, M. Li, *J. Phys. Chem. C* **2020**, *124*, 6145.
[25] S. Wang, T. Kou, J. B. Varley, S. A. Akhade, S. E. Weitzner, S. E. Baker, E. B. Duoss, Y. Li, *ACS Mater. Lett.* **2021**, *3*, 100.
[26] T. Dou, Y. Qin, F. Zhang, X. Lei, *ACS Appl. Energy Mater.* **2021**, *4*, 4376.
[27] W. J. Dong, I. A. Navid, Y. Xiao, J. W. Lim, J.-L. Lee, Z. Mi, *J. Am. Chem. Soc.* **2021**, *143*, 10099.
[28] K. R. Phillips, Y. Katayama, J. Hwang, Y. Shao-Horn, *J. Phys. Chem. Lett.* **2018**, *9*, 4407.
[29] Y. Deng, Y. Huang, D. Ren, A. D. Handoko, Z. W. Seh, P. Hirunsit, B. S. Yeo, *ACS Appl. Mater. Interfaces* **2018**, *10*, 28572.
[30] D. Yang, S. Zuo, H. Yang, X. Wang, *Adv. Energy Mater.* **2021**, *11*, 2100272.
[31] W. Zhu, L. Fan, Q. Geng, C. Wang, X. Fan, Y. Zhang, C. Li, *Chem. Eng. J.* **2024**, *489*, 151316.
[32] S. Liang, Z. Fang, C. Yang, Q. Wang, *Chem. Commun.* **2024**, *60*, 7602.
[33] S. Liang, J. Xiao, T. Zhang, Y. Zheng, Q. Wang, B. Liu, *Angew. Chem., Int. Ed.* **2023**, *62*, e202310740.
[34] P. Roy, S. K. Srivastava, *CrystEngComm* **2015**, *17*, 7801.
[35] U. Shamraiz, R. A. Hussain, A. Badshah, *J. Solid State Chem.* **2016**, *238*, 25.
[36] C. Balischewski, H.-S. Choi, K. Behrens, A. Beqiraj, T. Körzdörfer, A. Geßner, A. Wedel, A. Taubert, *ChemistryOpen* **2021**, *10*, 272.
[37] S. Sun, P. Li, S. Liang, Z. Yang, *Nanoscale* **2017**, *9*, 11357.
[38] P. V. Quintana-Ramirez, M. C. Arenas-Arrocena, J. Santos-Cruz, M. Vega-González, O. Martínez-Alvarez, V. M. Castaño-Meneses, L. S. Acosta-Torres, J. de la Fuente-Hernández, *Beilstein J. Nanotechnol.* **2014**, *5*, 1542.
[39] A. Abouserie, G. A. El-Nagar, B. Heyne, C. Günter, U. Schilde, M. T. Mayer, S. Stojkovikj, C. Roth, A. Taubert, *ACS Appl. Mater. Interfaces* **2020**, *12*, 52560.
[40] J. Llopis, J. M. Gamboa, L. Arizmendi, *Electrochim. Acta* **1961**, *4*, 294.
[41] M. Urbanová, J. Kupčík, P. Bezdička, J. Šubrt, J. Pola, *C. R. Chim.* **2012**, *15*, 511.
[42] C. H. M. van Oversteeg, M. Tapia Rosales, K. H. Helfferich, M. Ghiasi, J. D. Meeldijk, N. J. Firet, P. Ngene, C. de Mello Donegá, P. E. de Jongh, *Catal. Today* **2021**, *377*, 157.
[43] Y. Huang, Y. Deng, A. D. Handoko, G. K. L. Goh, B. S. Yeo, *ChemSusChem* **2018**, *11*, 320.
[44] T. Shinagawa, G. O. Larrazábal, A. J. Martín, F. Krumeich, J. Pérez-Ramírez, *ACS Catal.* **2018**, *8*, 837.
[45] F. Scholten, I. Sinev, M. Bernal, B. R. Cuenya, *ACS Catal.* **2019**, *9*, 5496.
[46] L. C. Pardo Pérez, A. Arndt, S. Stojkovikj, I. Y. Ahmet, J. T. Arens, F. Dattila, R. Wendt, A. Guilherme Buzanich, M. Radtke, V. Davies, K. Höflich, E. Köhnen, P. Tockhorn, R. Golnak, J. Xiao, G. Schuck, M. Wollgarten, N. López, M. T. Mayer, *Adv. Energy Mater.* **2021**, *12*, 2103328.
[47] G. A. El-Nagar, F. Yang, S. Stojkovikj, S. Mebs, S. Gupta, I. Y. Ahmet, H. Dau, M. T. Mayer, *ACS Catal.* **2022**, *12*, 15576.
[48] Z.-H. Ge, B.-P. Zhang, Y.-X. Chen, Z.-X. Yu, Y. Liu, J.-F. Li, *Chem. Commun.* **2011**, *47*, 12697.
[49] L. Liu, B. Zhou, L. Deng, W. Fu, J. Zhang, M. Wu, W. Zhang, B. Zou, H. Zhong, *J. Phys. Chem. C* **2014**, *118*, 26964.
[50] E. N. Selivanov, R. I. Gulyaeva, A. D. Vershinin, *Inorg. Mater.* **2007**, *43*, 573.
[51] M. Miloshova, D. Baltes, E. Bychkov, *Water Sci. Technol.* **2003**, *47*, 135.
[52] V. G. Celante, M. B. J. G. Freitas, *J. Appl. Electrochem.* **2010**, *40*, 233.
[53] Y. S. Chu, I. K. Robinson, A. A. Gewirth, *J. Chem. Phys.* **1999**, *110*, 5952.
[54] H.-H. Huang, *Metals* **2016**, *6*, 23.
[55] M. C. Biesinger, *Surf. Interface Anal.* **2017**, *49*, 1325.
[56] NIST X-ray Photoelectron Spectroscopy Database (SRD 20), Version 5.0, https://dx.doi.org/10.18434/T4T88K (accessed: August 2024).
[57] S. A. Awe, J.-E. Sundkvist, Å. Sandström, *Miner. Eng.* **2013**, *53*, 39.
[58] K. Yang, R. Kas, W. A. Smith, *J. Am. Chem. Soc.* **2019**, *141*, 15891.
[59] Y. Wang, H. Xu, Y. Liu, J. Jang, X. Qiu, E. P. Delmo, Q. Zhao, P. Gao, M. Shao, *Angew. Chem., Int. Ed.* **2024**, *63*, 202313858.